

# Vision-Based Adaptive Robotics for Autonomous Surface Crack Repair

Joshua Genova<sup>a</sup>, Eric Cabrera<sup>b</sup>, Vedhus Hoskere<sup>a,c,\*</sup>

<sup>a</sup> *Department of Electrical and Computer Engineering, University of Houston, 4226 MLK Blvd, Houston, TX 77204, United States*

<sup>b</sup> *Department of Mechanical Engineering, University of Houston, 4226 MLK Blvd, Houston, TX 77204, United States*

<sup>c</sup> *Department of Civil and Environmental Engineering, University of Houston, 4226 MLK Blvd, Houston, TX 77204, United States*

\* Corresponding author at: Department of Civil and Environmental Engineering, University of Houston, 4226 MLK Blvd, Houston, TX 77204, United States

E-mail addresses: [jtgenova@cougarnet.uh.edu](mailto:jtgenova@cougarnet.uh.edu) (J. Genova), [vhoskere@central.uh.edu](mailto:vhoskere@central.uh.edu) (V. Hoskere).

## Abstract

Surface cracks in infrastructure can lead to significant deterioration and costly maintenance if not efficiently repaired. Manual repair methods are labor-intensive, time-consuming, and imprecise and thus difficult to scale to large areas. While advancements in robotic perception and manipulation have progressed autonomous crack repair, existing methods still face three key challenges: (i) accurate localization of cracks within the robot's coordinate frame, (ii) adaptability to varying crack depths and widths, and (iii) validation of the repair process under realistic conditions. This paper presents an adaptive, autonomous system for surface crack detection and repair using robotics with advanced sensing technologies to enhance precision and safety for humans. The system uses an RGB-D camera for crack detection, a laser scanner for precise measurement, and an extruder and pump for material deposition. To address one of the key challenges, the laser scanner is used to enhance the crack coordinates for accurate localization. Furthermore, our approach demonstrates that an adaptive crack-filling method is more efficient and effective than a fixed-speed approach, with experimental results confirming both precision and consistency. In addition, to ensure real-world applicability and testing repeatability, we introduce a novel validation procedure using 3D-printed crack specimens that accurately simulate real-world conditions. This research contributes to the evolving field of human-robot interaction in construction by demonstrating how adaptive robotic systems can reduce the need for manual labor, improve safety, and enhance the efficiency of maintenance operations, ultimately paving the way for more sophisticated and integrated construction robotics.

*Keywords:*

Robotics

Infrastructure maintenance

Crack repair

Adaptive repair

End-effector design

Computer vision

## 1. Introduction

In the field of infrastructure maintenance, the efficient detection and repair of surface cracks represents one of the most persistent and challenging problems. Surface cracks are typically non-structural but can lead to long-term deterioration due to moisture or chemical ingress. Over time, these minor imperfections may propagate and become structurally significant, potentially leading to costly repairs or even catastrophic failures. Traditional methods for crack repair, such as pouring, filling, sealing, pressure pouring, and banded digging-patching [1], rely heavily on manual labor and often result in inconsistent repair quality while posing major safety risks. Additionally, manual crack repair can be a time-consuming process that can cause significant delays to the recovery of communities affected. For example, from 2016 to 2018, surface crack repair in San Francisco International Airport runways cost close to half a million dollars directly, and

millions more in economic impact due to the 1,103 flights that were cancelled and the 13,217 flights that were delayed during repair days [2]. As another example, in the aftermath of earthquakes such as the 2011 Christchurch earthquake, inspection and repair efforts can take weeks, months, or even years due to a lack of manpower and inaccessibility [3,4]. These statistics emphasize the noteworthy benefits that could be unlocked by timely, efficient, and proactive surface crack detection and repair that prevent such economic losses and disruptions.

Robotic systems can help improve repair processes by significantly reducing repair times and minimizing associated risks in such scenarios. However, for these systems to be truly effective, they must be capable of being adaptive to human input on the field while also functioning adaptively to autonomously sensed conditions such as varying crack sizes and conditions. This adaptability is crucial in ensuring an efficient and effective repair. Fig. 1 shows examples of cracks in an airport runway being repaired manually by human experts, a building wall post-earthquake, and unsightly crack on top of a door.



**Fig. 1.** Surface cracks in different environments: an airport runway under repair (left), a building wall post-earthquake (middle), and a crack above a door (right).

Research on robotic repair of infrastructure has been very limited. However, researchers have made relevant progress in two directions: (i) robotic perception and (ii) robotic manipulation. Research on robotic perception of cracks has focused mainly on crack detection and measurement [5–28]. On the other hand, robotic manipulation for crack filling involves developing advanced end-effectors and control methods in the application of repair materials to identified cracks [29–37].

Recent advancements in crack detection and measurement have introduced a variety of innovative systems aimed at enhancing automation and accuracy of crack quantification. Hoskere discussed approaches for development of datasets for automated identification damage such as cracks using deep learning [5]. Research has also focused on infrastructure inspection deploying high-resolution sensors and cameras, frequently mounted on UAVs, automated guided vehicles (AGVs), or robotic manipulators [6–12]. For example, Khan et al. developed an automated pavement crack inspection system using a mobile robot with an RGB camera to survey predefined areas [13]. Additionally, many researchers have concentrated on computer vision and deep learning approaches for the detection and segmentation of cracks [14–18]. For instance, Wang et al. introduced a dual-path network combining a lightweight CNN and a transformer encoder, achieving superior crack segmentation performance on multiple datasets [19]. Moreover, Dong et al. proposed a novel multilayer feature association fusion network (MFAFNet) that significantly enhances crack segmentation accuracy and efficiency in asphalt pavements [20]. Multi-sensor systems, utilizing combinations of RGB-D cameras, laser scanners, and LiDAR, have achieved improved accuracy in quantifying sub-millimeter cracks [21–25]. As an example, Alamdari et al. presented a multi-sensor robotic approach that combines convolutional neural networks, laser scanning, and LiDAR-based 3D point cloud to detect and quantify hairline cracks in concrete structures, capable of measuring crack widths smaller than 0.01 mm [26]. Furthermore, Hu et al. developed a LiDAR and camera data fusion with a crack segmentation network and quantification, achieving 3D autonomous crack detection with geometric errors of less than

0.1 mm from the ground truth. [27]. While these studies have demonstrated success in automated inspection, crack detection, and measurement, the logical progression is to move from detection to the actual repair of cracks. During crack detection and quantification, accurate localization is not of concern as the robot does not need to target the exact center points of the crack. Effective repair on the other hand relies not only on detection, but also on localizing cracks within the robotic repair system's coordinate frame to submillimeter accuracy, a challenge that remains underexplored. Chen et al. developed a semi-autonomous vision-guided system for crack filling that uses an RGB-D camera for crack localization [28]. However, their system frequently resulted in large errors of over 10s of mm in all directions causing the need for manual intervention for correction. Therefore, integrating advanced perception systems capable of accurately localizing crack coordinates will significantly enhance the effectiveness and reliability of autonomous crack repair solutions.

In the realm of robotic crack repair, various advanced tools and end-effectors have been developed to fill cracks of known size and location. Awuah et al. modified a 3D printer to be able to dispense bitumen to repair cracks in asphalt concrete in a lab setting [29]. In a similar manner, the Self Repairing Cities project utilized 3D printing technology on a UAV by equipping it with a nozzle mounted on a delta arm, adapted from a commercial 3D printer [30]. To further enhance accessibility in hard-to-reach areas, soft continuum arms have also been integrated with UAVs [31,32]. However, UAV mounted crack filling systems struggle with precise targeting of cracks and have limited payload capacity. In addition to these approaches, robotic end-effectors mounted on robotic manipulators offer promising solutions for autonomous crack repair for more accessible structures. For example, Pereira et al. developed an end-effector for robotic manipulator that monitors and controls sealing quality by measuring contact force and using computer vision to measure the width of the sealant [33]. While these methods have made significant advancements, they would not be able to account for cracks of varying widths and depths, resulting in underfilling or overfilling for variable crack sizes often observed in the real world. Zhu et al. designed a manipulator capable of adapting to varying crack depths, although their system was limited to measuring height differences between the end-effector and the crack, without addressing the actual crack-filling process [34], and doesn't account for varying crack widths. Implementing sensor feedback to control the robotic system's material flow could enable precise and effective crack repair across diverse geometries.

Evaluating developed crack filling procedures can be challenging as they require the robotic system, crack filling material, and an environment where tests can be repeated. As a result, researchers have come up with various analogues filling to test and validate developed systems for robotic crack repair. For instance, Veeraraghavan et al. developed a mobile robot equipped with a nozzle at its base to fill cracks within the robot's footprint but, their approach was validated using paint droplets on drawn cracks [35]. Similarly, Schaefer et al. designed a syringe-like end-effector that was tested on a simulated crack by taping two halves of cementitious mortar together and manually filling the gap with a user-defined trajectory [36]. In addition, Rahman et al. created an inspection and repair system with a robotic arm mounted on an AGV, but their system's repair sequence only simulated the motion of repairing a crack without dispensing filling material [37]. While these efforts represent significant progress, the validation of successful crack filling under realistic conditions remains insufficiently addressed. Demonstrating repair motions or testing in simulated environments does not fully capture a system's effectiveness. Furthermore, it is crucial to ensure that the quality of the filled crack is assessed to confirm successful repair. Developing a repeatable testbed for evaluating the efficacy of crack-repair methods can help develop robotic maintenance systems.

In summary, despite progress in robotic perception and manipulation, three key technical challenges persist: (i) accurate localization of cracks within the robot's coordinate frame, (ii) adaptability of the filling process to account for variations in crack depth and width, and (iii) validation of the crack repair process through a controlled and repeatable testing environment. Accurate localization of the crack in 3D robot coordinate system is necessary for the robot to navigate to the crack center points and execute the filling process correctly. Furthermore, an adaptive system is necessary for accommodating the diverse dimensions of

cracks, including their varying widths and depths. Failure to adjust to these differences can lead to inadequate filling, resulting in early deterioration, poor adhesion, excessive material waste, and visually unappealing repairs. In addition, many systems, although precise in simulated environments, lack extensive real-world testing and validation, particularly in dynamic and practical conditions such as changing lighting and filler rheology. Our research aims to address these three challenges by developing a comprehensive, end-to-end, adaptive, and autonomous system that enhances robotic capabilities and optimizes the collaboration between human operators and robots, ensuring accuracy and reliability in practical applications. While humans excel in making judgment calls and identifying potential problem areas, robots are more efficient and precise in executing repetitive tasks like crack filling, making the combination of human intuition and robotic precision a powerful approach to infrastructure maintenance.

This paper discusses a novel methodology for crack-repair that addresses both crack detection and repair with high precision. The three novel contributions of our research are:

- i. Framework for human-robot interaction for crack repair
- ii. Novel computer vision pipeline that enables accurate crack localization in the robot coordinate system and simultaneous crack measurement using RGB-D camera-laser scanner setup
- iii. An autonomous and adaptive crack filling system using a robotic arm and custom end-effector that integrates detection, measurement, and repair for various crack sizes.
- iv. A repeatable validation procedure using a 3D printed crack that compares scans before and after filling.

To demonstrate our contributions, we conduct tests in both simulation and in the laboratory environment by constructing the proposed system.

The remainder of this paper is organized as follows: Section 2 describes the framework for human-robot interaction for crack repair. Section 3 presents the proposed methodology for crack repair, covering calibration, crack coordinates extraction from image to coordinates, coordinates enhancement and crack profile measurement using a laser scanner, and the crack filling process. Section 4 describes the simulation environment and experimental setup, including the overall system design. Section 5 presents the results of material extrusion calibration, the use of adaptive speed versus constant speed during crack filling, and the comparison between sensors for localization accuracy. Finally, Section 6 concludes the paper.

## **2. Framework for Human-Robot Interaction for Crack Repair**

We now describe our proposed framework for human-robot interaction for surface crack repair. The rationale behind the framework is to leverage the strengths of both human and robotic capabilities to enhance the accuracy, efficiency, and safety of surface crack repair. Humans are better at making high-level decisions such as which cracks need to be repaired. However, the detection and accurate measurement of cracks for crack filling would be too cumbersome when many cracks are present, and the process of executing crack filling can be very laborious and affect human's health long term. On the other hand, different robotic systems can tirelessly collect data and accurate sensing systems can be deployed on these robots depending on the fidelity of data to be collected. [Fig. 2.](#) illustrates proposed framework in a surface crack repair environment: it begins with a UAV mapping a room and scanning for cracks, followed by an automated crack detection algorithm. The cracks are localized based on the map developed and an approximate location is associated with each crack. Based on the collected data, a human operator can evaluate the urgency of repairs and select which cracks to address. The operator then commands the robotic system via a wireless connection to navigate to the selected crack location manually. Once the robot is at the correct crack, the human then verifies the crack and then orders the robot to initiate the filling process. Then, the robot autonomously makes accurate measurements to localize the crack in its local coordinate system, and then executes an adaptive fill procedure without any human intervention. This collaborative approach not only improves the efficiency of the crack repair process, but also minimizes disruptions and

ensures that human workers can operate safely and effectively alongside advanced robotic systems. The rest of this paper focuses specifically on the method for crack repair once the human has identified the crack, ultimately leading to an autonomous and adaptive repair process.

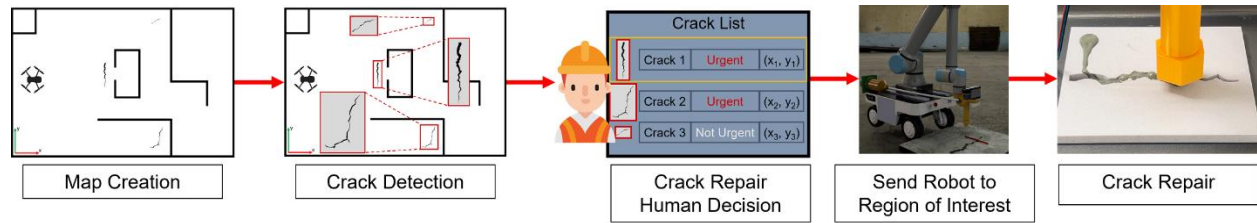


**Fig. 2.** Framework for human-robot interaction for surface crack repair.

### 3. Proposed Methodology for Crack Repair

This section outlines our proposed system and methodology for crack repair. Our methodology consists of four parts (i) extrusion calibration, (ii) crack coordinates extraction, (iii) crack profile, and (iv) crack filling. Fig. 3 illustrated the methodology through a high-level system overview. The proposed methodology begins with a calibration process where material is printed at various speeds and measured to determine extrusion rates. Next, crack coordinates are extracted using an image to segment the crack via a pre-trained model, extracting centerline pixels, and transforming them into robot coordinates. Subsequently, the system refines these coordinates with a laser scanner, enhancing precision and measuring the cross-sectional area to adjust the robot's speed for accurate filling. The crack filling process then begins where material is pumped from a custom-designed, 3D-printed pump to the print head, extruded at a constant flow rate, which is driven by a microprocessor. The robot moves to the coordinates at assigned speeds to ensure precise filling. Finally, we discuss the proposed validation methodology through a rescan for post-fill profiles, applying heuristic algorithms to detect cross-sectional area, and ensuring the crack is properly repaired.

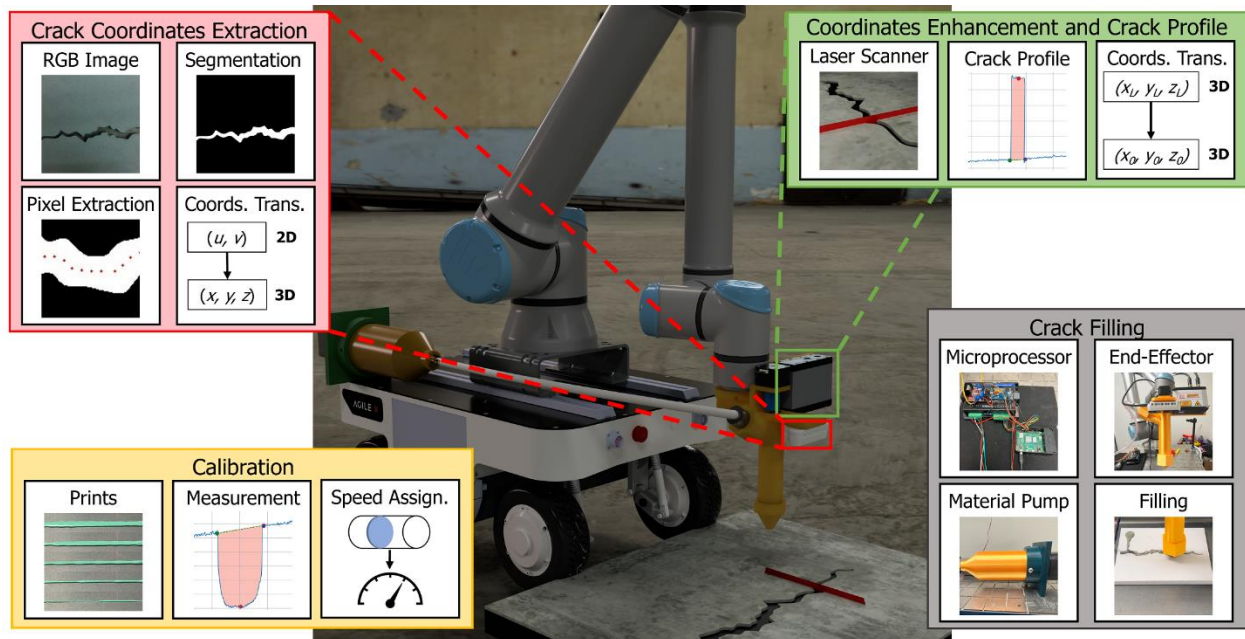


**Fig. 3.** High-Level System Overview.

### 3.1 Extrusion Calibration

The calibration process is crucial for ensuring accurate material extrusion during crack repair. However, the rheology of the crack filler mixture presents challenges that are not the focus of this project. We strive to maintain consistent mixture properties for every experiment, but variations can occur due to several factors. One challenge is the reuse of the material; since the proportions of clay and water in the reused material are not precisely known, we add more until we achieve an ideal consistency. Additionally, heat and humidity can affect the mixture's properties. To reduce costs, we save and reuse as much material as possible after each experiment. Therefore, the calibration process is essential for determining the extrusion rate at different speeds, ensuring reliable and accurate material deposition. To begin, we print a strip of material at different speeds and measure the cross-sectional area with the laser scanner. The laser scanner provides 2D measurements, with the x-axis representing the width of the scanned line and the y-axis representing the distance from the laser scanner. To calculate the actual width and height of the print, we employ a heuristic algorithm. First, we identify the indices with the largest rate of change, which indicate the edges of the printed material as shown in Eq. (1). A flat profile from the laser scanner data implies a flat surface with no print. The cross-sectional area  $A$  is then calculated by integrating the  $z$  values over the width, as shown in Eq. (2). The center of the profile is found by averaging these indices as depicted in Eq. (3) and Eq. (4). This process ensures precise measurements of the height and cross-sectional area of the printed material, which are essential for accurate material extrusion during the crack repair process.

$$x_1 = \mathbf{x}[i_1]; \quad x_2 = \mathbf{x}[i_2] \tag{1}$$

$$A = \int_{x_1}^{x_2} z dx \approx \sum_{i=i_1}^{i_2} \mathbf{z}[i] \Delta x \tag{2}$$

$$i_{avg} = \frac{i_1 + i_2}{2} \tag{3}$$

$$(c_x, c_y) = (\mathbf{x}[i_{avg}], \mathbf{z}[i_{avg}]) \tag{4}$$

Where  $x_1$  and  $x_2$  are the  $x$  value from the laser scanner data at  $i_1$  and  $i_2$ , the two indices with the largest sudden change of the laser depth  $z$ ,  $A$  is the cross-sectional area,  $\Delta x$  is the change between the  $x$  values,  $i_{avg}$  is the average of the two indices, and  $c_k$  is the center position of the crack in the  $k$  axis.

### 3.2 Crack Coordinates Extraction

After calibration, 3D crack coordinates are extracted to allow for automated navigation of the robot along the length of the crack. The crack coordinate extraction process begins by detecting cracks using a segmentation model applied on RGB images, followed by extracting centerline pixel coordinates through skeletonization. These pixels are then transformed from camera coordinates to robot coordinates using the pin-hole camera model, and the final path is optimized using a heuristic approach. This section details the methods used for detecting cracks and transforming the detected coordinates into format that the robot can interpret and use.

#### 3.2.1 Crack Detection using CNN and Stereo Depth Camera

Accurate crack detection is the foundation of our proposed repair process. We start with the assumption that the robot has already been moved so that a crack is visible in the frame of the RGB-D camera. Then, an image is captured, and a crack segmentation algorithm is applied. Our pipeline is agnostic to the specific crack segmentation method utilized. In this paper, we apply a pretrained DeepLabV3+ model, trained on

the conglomerate crack dataset containing over 10,000 images [38–43]. The captured RGB image is fed into the DeepLabV3+ model, which segments the crack and outputs a black-and-white image mask highlighting the crack. Fig. 4 illustrates this process: The first row of the figure shows the original RGB image, the second row displays the segmented mask, and the last row demonstrates the overlay of the segmentation on top of the original RGB image. This overlay helps in visually assessing the model’s segmentation performance. By integrating the RGB-D camera with the advanced DeepLabV3+ model, we achieve a robust and accurate crack detection system, forming the basis for the subsequent stages of the repair process.

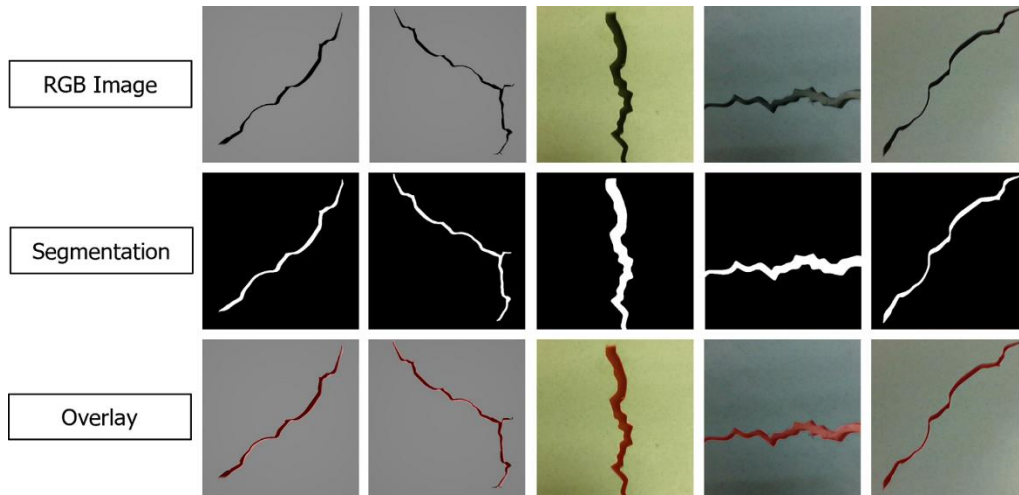


Fig. 4. Image Capture and Segmentation.

### 3.2.2 Image Pixel Extraction

With the mask image from the segmentation model, we proceed to extract the pixel coordinates of the crack as depicted in Fig. 5. First, we convert the segmented mask image to grayscale to simplify the data, ensuring that the crack stands out against the background. We then apply a binary threshold to the grayscale image, creating a clear black-and-white binary image where the crack is distinctly represented. Next, we perform skeletonization on the binary image. Skeletonization is a morphological operation that iteratively removes outer pixels of the crack representation, reducing it to its thinnest form while preserving the overall structure [44]. This operation results in a one-pixel-wide skeleton that accurately traces the central path of the crack, providing a precise and simplified representation for subsequent steps. After skeletonization, we extract the coordinates of the skeleton pixels, representing the exact path of the crack. To manage the data effectively, we simplify the coordinates by filtering out points that are too close to each other based on a predefined threshold. This filtering ensures that the dataset is both accurate and efficient, facilitating easier transformation into 3D coordinates for the robotic system's navigation and repair tasks.

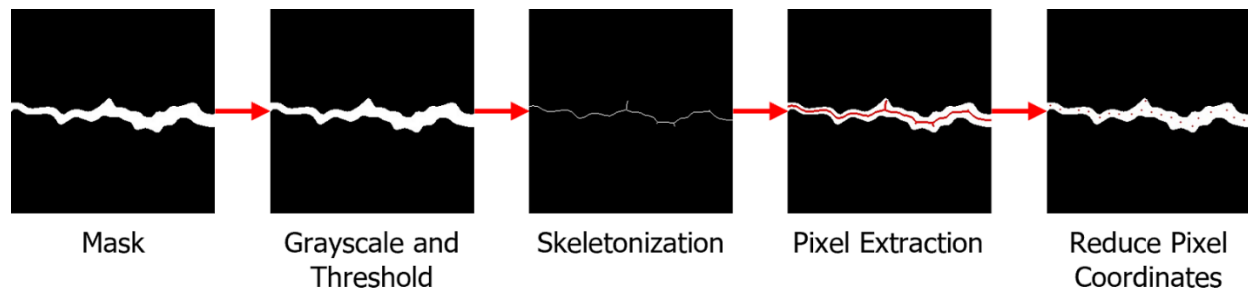


Fig. 5. Pixel Coordinate Extraction Process.

### 3.2.3 Pin-Hole Camera Model

To accurately transform the pixel coordinates of detected cracks into 3D camera coordinates, we use the pin-hole camera model illustrated in Fig. 6. This model is essential because it translates the 2D image data captured by the RGB-D camera into a spatial format that the robot can use. This transformation allows the robotic system to understand the exact position and orientation of the cracks in the real world, enabling precise and effective repair operations. The pin-hole camera model shows how a point  $P(X, Y, Z)$  in the 3D world is projected onto the image plane at point  $p$  [45]. The principal point  $(x, y)$  is the projection of the center of the camera onto the image plane, and the distance  $f$  represents the focal length. The center of projection, where all projection lines converge, represents the optical center of the camera. The intrinsic camera parameters are encapsulated in the  $\mathbf{K}$  matrix, as shown in Eq. (5). These parameters include the focal lengths ( $f_x$  and  $f_y$ ) and the optical center or principal point  $(p_x, p_y)$ . The intrinsic matrix  $\mathbf{K}$  is critical for accurately mapping the 2D pixel coordinates to 3D space. The transformation from pixel coordinates to camera coordinates is illustrated by Eq. (6), where the Camera Coordinates represent the 3D points in the camera's coordinate system,  $\mathbf{K}$  is the intrinsic matrix, and Pixel Coordinates  $(u, v)$  are the 2D points from the segmented image, with  $z_c$  being the respective depth values obtained from the RGB-D camera.

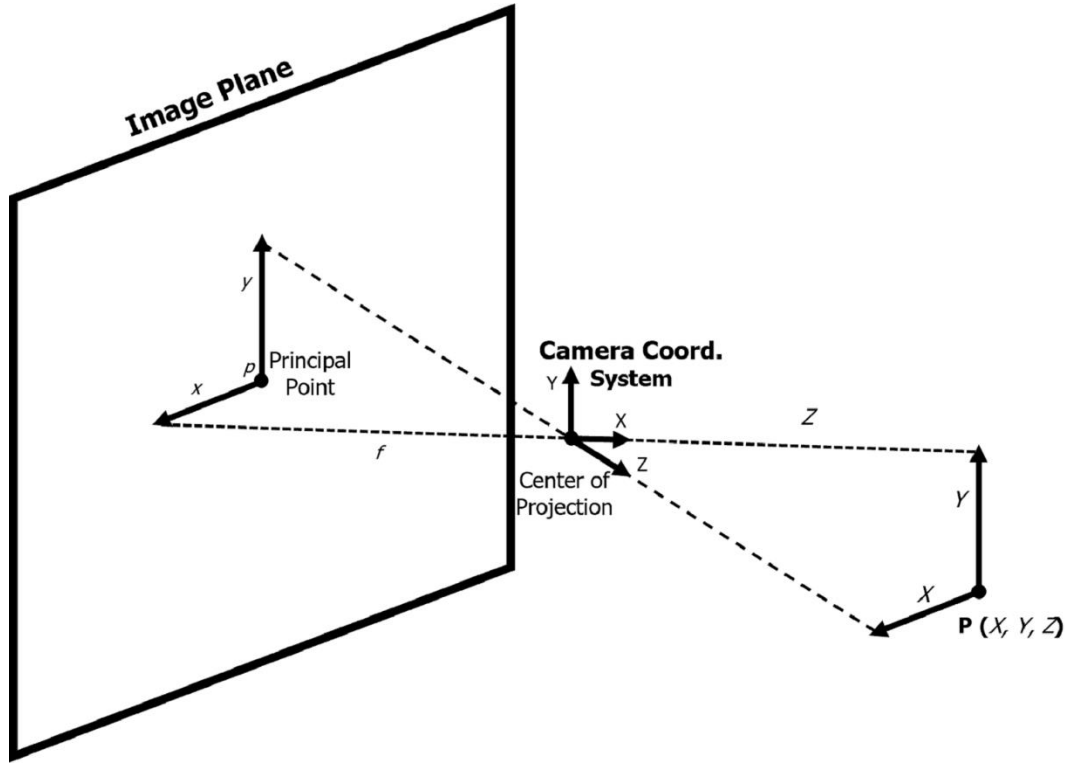


Fig. 6. Pin-Hole Camera Model.

$$K = \begin{bmatrix} f_x & 0 & p_x \\ 0 & f_y & p_y \\ 0 & 0 & 1 \end{bmatrix} \quad (5)$$

$$\begin{bmatrix} x_c \\ y_c \\ z_c \end{bmatrix} = \mathbf{K}^{-1} * z_c * \begin{bmatrix} u \\ v \\ 1 \end{bmatrix} \quad (6)$$



### 3.2.4 Transformation from Camera Coordinates to Robot Coordinates

Robot coordinates are then computed from the camera coordinates. We create a transformation matrix that converts the camera coordinates into the robot base's reference frame using the camera's extrinsic parameters, including its translation and rotation relative to the robot's base using the robot's API. The transformation from camera coordinates to robot base coordinates is defined by Eq. (7), where  $T_0^C$  is the transformation matrix. Fig. 7 illustrates the overall process, from pixel coordinates to robot base coordinates. The origin in the image plane, depicted by  $O_{image}$ , is where the pixel coordinates of the crack are located. The crack coordinates in the image plane are then transformed to camera coordinate system using the approach discussed previously, resulting in a new origin,  $O_{camera}$ . Subsequently,  $O_{camera}$  is transformed into  $O_{robot}$ , which is the origin of the robot base frame, thereby converting the crack coordinates in the camera coordinate system to the robot base coordinate system. By transforming the camera coordinates to robot coordinates, the robotic system can interpret and act upon the spatial positioning of the cracks, ensuring accurate and effective repair operations.

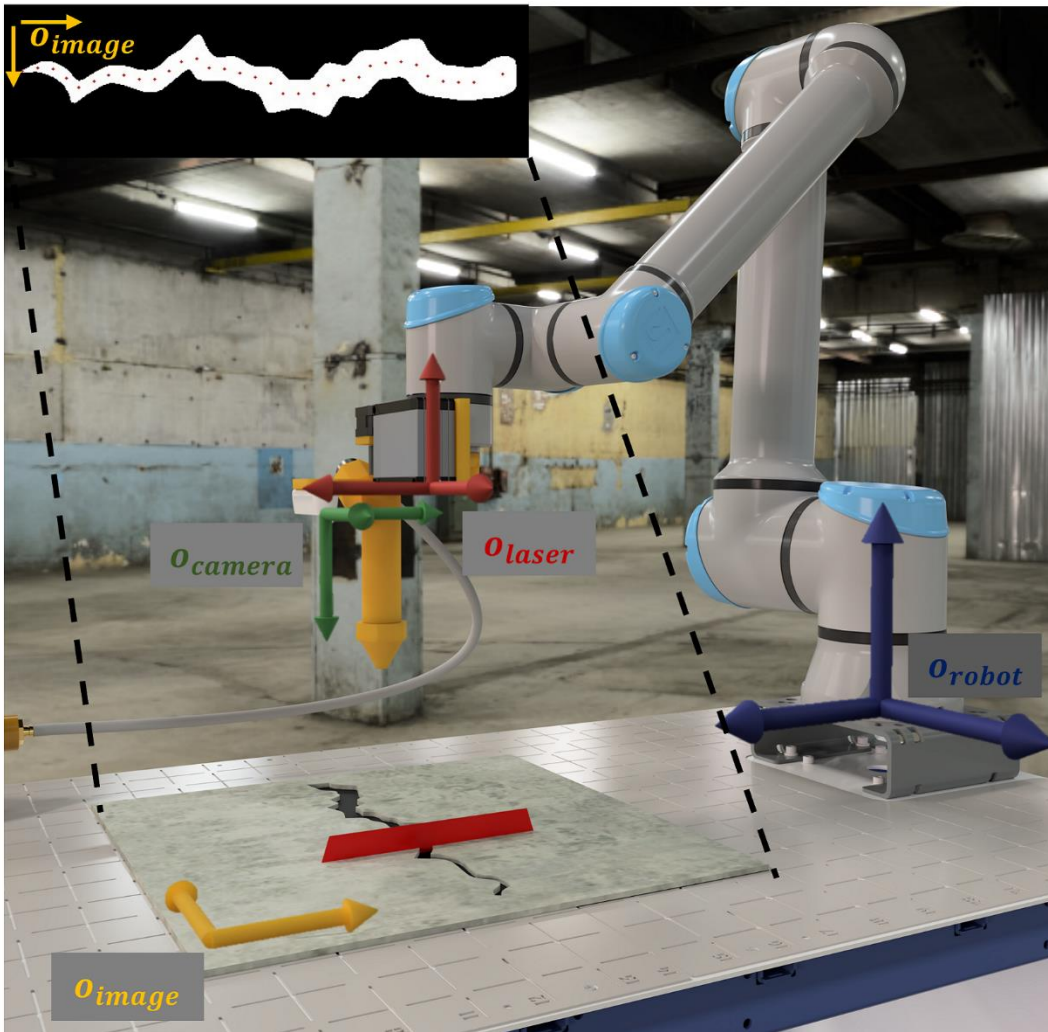


Fig. 7. Transformation from 2D Image Coordinates to 3D Robot Base Coordinates.

$$\begin{bmatrix} x_0 \\ y_0 \\ z_0 \end{bmatrix} = T_C^0 * \begin{bmatrix} x_c \\ y_c \\ z_c \end{bmatrix} \quad (7)$$

### 3.2.5 Path Optimization using Heuristic Approach

Once the crack coordinates have been transformed into the robot's coordinate system, the next step is to optimize the path for the robot to follow during the repair. Using a heuristic approach, we aim to minimize travel distance, ensure complete coverage, and avoid redundant movements. After the image pixel extraction, the robot coordinates are stored in random order. To optimize the path, the algorithm first calculates the maximum distances between the x and y coordinates. Depending on which distance is greater, the coordinates are sorted along either the x or y axis, ensuring efficient navigation along the crack. While other path optimization algorithms, such as the Two-Opt Algorithm, Genetic Algorithm, and Held-Karp Algorithm, were considered, the heuristic approach proved sufficient for the generally horizontal and vertical crack patterns tested in this paper. For more complex patterns, like diagonal or branching cracks, more advanced algorithms may be necessary. By employing this heuristic approach, we enhance the robot's efficiency and precision, reducing time and material usage while maintaining high repair quality.

## 3.3 Coordinates Enhancement and Crack Profile

In this section, we describe the methods used to enhance the initial image-based crack coordinates and generate accurate crack profiles. While the RGB-D camera provides valuable initial data, its depth measurements often suffer from significant errors. This limitation results in crack coordinates that lack the precision needed for accurate localization in 3D space, which is crucial for effective robotic navigation. To address this issue, a laser scanner is integrated into the system. The new RGB-D camera-laser scanner significantly enhances the accuracy of the crack coordinates by providing high-resolution data that precisely maps the crack's geometry. This enhancement is essential not only for precise robot navigation but also for generating detailed crack profiles. Accurate crack profiles are also vital for determining the cross-sectional area at each coordinate, which in turn helps to identify the appropriate speed needed for optimal material extrusion.

### 3.3.1 Laser Scanning, Data Acquisition, and Profile Generation

To enhance the accuracy of the initially detected crack coordinates, we use a laser scanner to capture high-resolution data along the crack. The laser scanner projects a line of laser light onto the surface and captures the reflected light to measure the distance accurately, generating detailed 2D profiles at regular intervals. The same heuristic algorithm is used from the calibration process to generate the profile of the crack. The main difference is instead of height of the print, we have the depth of the crack. The result is a cross-sectional profile of the crack, which is necessary for planning the material deposition during the repair process. By generating accurate crack profiles, we can correlate which robot speed is needed at specific crack coordinates to properly fill the crack at that point.

### 3.3.2 Transformation from Laser Coordinates to Robot Coordinates

The crack coordinates from the laser scanner coordinate systems are then transformed to the robot coordinate system. The center point of the crack in laser coordinates is obtained from the profile using the algorithm described in Eq. (4). The center x-coordinate,  $c_x$  shows how far the original point is from the true center of the crack on its x-axis, or y-axis depending on the crack pattern, with a value of 0 indicating the exact center. The center y-coordinate,  $c_y$  from represents the distance of the laser scanner from the center of the crack on its z-axis. Depending on the crack pattern, Eq. (8) for horizontal crack, and Eq. (9) for vertical cracks. This information is used to correct the previous robot coordinates using Eq. (10), transforming into the robot base's reference frame using a transformation matrix,  $T_L^0$ . This matrix, derived from the laser scanner's translation and rotation parameters obtained via the robot's API, is applied to the center coordinates to transform them into the robot base coordinates. Fig. 7 illustrates the transformation from the laser coordinate system origin  $o_{laser}$  to the robot base coordinate system  $o_{robot}$ .

$$\text{Horizontal Cracks} \begin{cases} x_L = c_x \\ y_L = 0 \\ z_L = c_y \end{cases} \quad (8)$$

$$\text{Vertical Cracks} \begin{cases} x_L = 0 \\ y_L = c_x \\ z_L = c_y \end{cases} \quad (9)$$

$$\begin{bmatrix} x_0 \\ y_0 \\ z_0 \end{bmatrix} = T_L^0 * \begin{bmatrix} x_L \\ y_L \\ z_L \end{bmatrix} \quad (10)$$

### 3.4 Crack Filling

With the accurate crack coordinates and profile, the robot can begin filling the crack. The filling material is pumped through a custom-designed pump to the end-effector, which features a print head that extrudes the filling material. In a similar manner to traditional 3D printing technology using Polylactic acid (PLA), some material is initially extruded at the start of the repair process to ensure a consistent flow and to clear any potential blockages in the nozzle. This initial extrusion helps to minimize any inconsistency in material output. Once the flow is consistent, the robot moves to the crack coordinates and begins the filling process. As the robot follows the optimized path along the crack, the extruder deposits the material precisely into the crack. Throughout the process, the robot speed is adjusted based on each crack coordinates' cross-sectional area. The larger the area, the slower the robot and vice versa. This ensures that the crack is filled efficiently and effectively, enhancing the durability and longevity of the repair.

### 3.5 Validation

After the crack filling process is completed, the laser scanner is used again to perform a post-fill scan of the repaired crack. The same heuristic algorithm used during the initial scanning and calibration processes is applied to the post-fill scan data to detect the width and depth or height of the filled crack. An under-filled point will have some depth, while an over-filled point will have some height. The pre-fill and post-fill profiles are compared to assess the effectiveness of the repair. The absolute normalized difference between the pre-fill and post-fill profiles is calculated to quantify the accuracy of the repair, as shown in Eq. (11). Here,  $A_{pre}$  represents the cross-sectional area of the crack before filling, while  $A_{post}$  represents the cross-sectional area of the filled crack at the exact same coordinate. A lower value means a more accurate and effective repair, demonstrating a surface close to flat. By following this validation process, we ensure that the repairs meet the desired quality standards, providing a reliable and efficient approach to automated crack repair. The fill error,  $\epsilon_{fill}$  is given by.

$$\epsilon_{fill} = \left| \frac{A_{post}}{A_{pre}} \right| \quad (11)$$

## 4. Simulation and Experimental Setup

To evaluate the performance and validate the functionality of our automated crack repair system, we employed both simulation and experimental setups. The simulation environment allowed us to test and refine the system in a controlled virtual setting, minimizing potential issues before real-world deployment. The experimental setup provided a realistic testing environment to ensure the system's practical applicability and effectiveness.

## 4.1 Simulation Setup using RoboDK

The simulation environment used in this project is RoboDK, chosen for its robust robot Python programming API, cost-effectiveness, and ease of integration with real robots [46]. Fig. 8 shows the RoboDK simulation environment with the robot and end-effector as well as the simulated view from the camera. Using the robot's Python API, we can simulate the robot's motion both in the virtual environment and in the real world. RoboDK also has the capability to simulate a camera, allowing us to debug the crack detection and automation of robot motion. Both the real RGB-D camera and the laser scanner have their own Python APIs, facilitating smooth integration and implementation of all components in the real world. This comprehensive simulation setup ensures that we can thoroughly test and validate the system's functionality before deploying it in a real-world scenario, thereby minimizing potential issues and optimizing performance.

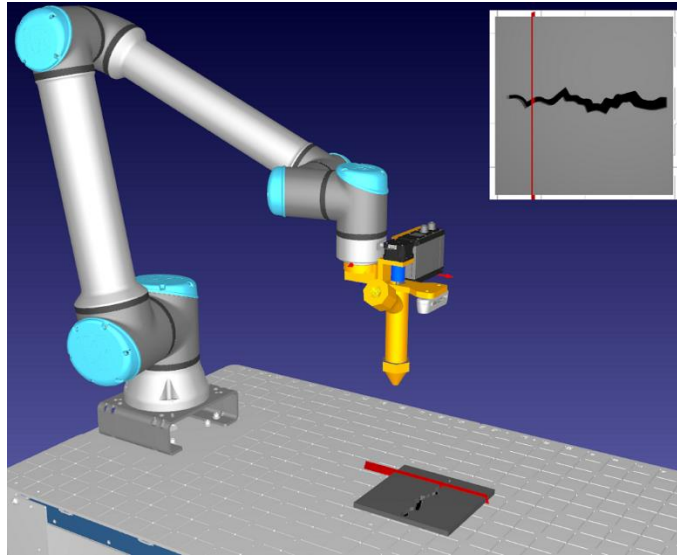


Fig. 8. RoboDK Simulation Environment.

## 4.2 Experimental Setup

The experimental setup involves the physical implementation of the automated crack repair system. This section details the complete system design, covering various components essential for the repair process. We will explore the design and functionality of the end-effector, which is crucial for material extrusion. Then, we provide a detailed overview of the pump design, underlining its integration with the overall system. Finally, we discuss the 3D-printed crack specimens, and the filling material used in the experiments, emphasizing their role in testing and validation.

### 4.2.1 System Design

The whole system design integrates various components essential for the automated crack repair process. Fig. 9 illustrates the complete setup, showcasing the interaction between the Universal Robot's UR10e robotic arm, end-effector, pump, microprocessor, and 3D-printed crack specimen. The UR10e robotic arm navigates along the crack and performs the repair with precision and a versatile reach, following the optimized path to deposit the repair material accurately. The print head, part of the end-effector, extrudes the filling material precisely into the crack, connected to the pump via tubing to ensure a steady flow. The custom-designed pump delivers the repair material from the reservoir to the print head, controlled by a microprocessor and motor drivers to maintain accurate flow rates. These microprocessor and motor drivers

manage the pump and extruder operations, controlling the constant flow of material. The 3D-printed crack specimen mimics real-world crack patterns, allowing for effective testing and validation of the repair process. This integrated design facilitates efficient and accurate crack repair, demonstrating the potential of the automated system in real-world applications.

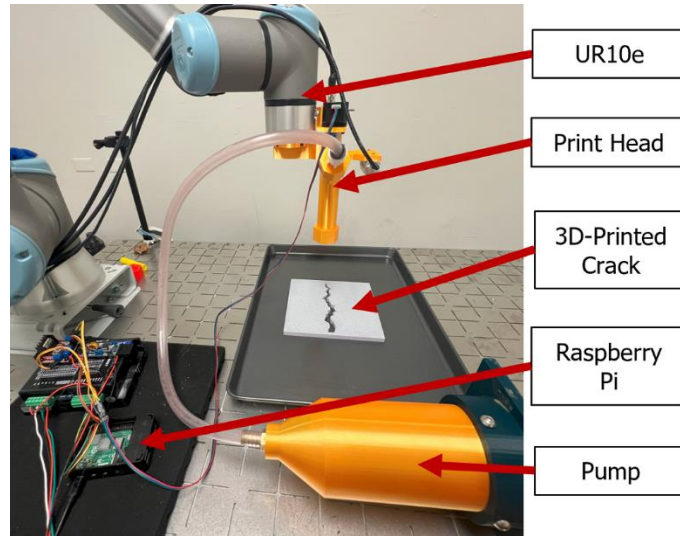


**Fig. 9.** System Design.

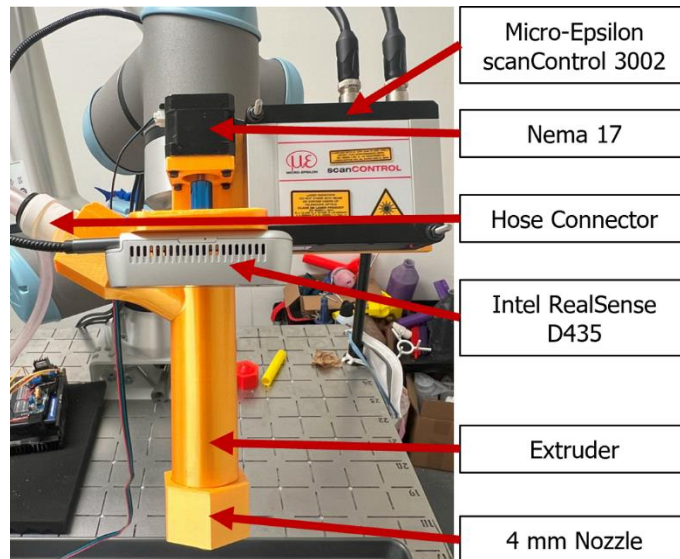


**Fig. 10.** End-Effector Design.

#### 4.2.2 End-Effector Design

The end-effector is a crucial component of the automated crack repair system, designed to dispense the repair material precisely into the crack. Fig. 10 showcases the custom-designed end-effector, which includes key components such as the Intel RealSense D435 RGB-D camera, the Micro-Epsilon scanControl 3002 laser scanner, and the print head. The RGB-D camera captures images of the crack, offering an RGB image resolution of 1920x1080 with a field of view of 69° x 42° and a depth range of 0.3-3 m with an error margin of 2%. The laser scanner enhances robot coordinates and creates detailed crack profiles, featuring a

measurement range of 200-420 mm in the z-axis, a resolution of 1024 points per profile, and a profile frequency of up to 10,000 Hz. The print head manages the material flow, delivered through flexible tubing to ensure consistent extrusion. The Nema 17 stepper motor drives an auger inside the print head, rotating to extrude the material through the 4 mm nozzle. This custom-designed end-effector ensures that the repair material is applied accurately and efficiently, contributing to the overall effectiveness and reliability of the crack repair system.

#### **4.2.3 Pump Design**

The pump system is designed to deliver material to the print head efficiently. It comprises 3D printed parts, a Nema 34 stepper motor, O-rings, barbed hose, and a threaded rod. The pump's design is heavily influenced by the structure of a medical syringe, featuring a cylinder-to-cone shape and a plunger mechanism that facilitates the extrusion of material from the pump to the hose and ultimately to the print head. The motor's movement, whether extending or retracting, controls the threaded rod, which in turn moves the piston. When the motor extends, the piston pushes the material inside the pump through the nozzle of the extruder via the tube. The efficiency of the pump is influenced by the diameter of the barbed hose and the viscosity of the material. A larger hose diameter and less viscous material typically results in a higher success rate of extrusion and flow. To improve the pump's performance, several modifications were made. The infill of the 3D printed pump was increased to enhance its structural integrity. Tolerances for the O-rings were minimized to prevent leakage, ensuring a reliable seal. Adjustments were made to handle different viscosities and types of materials, enhancing versatility. The design was refined to ensure the pump is safe and easy to use. Efforts were made to minimize material waste and enhance the overall efficiency of the extrusion process. These changes have collectively increased the pump's efficiency, durability, and user-friendliness, resulting in a more consistent extrusion system with minimal material waste.

#### **4.2.4 3D-Printed Crack and Filling Material**

To test and validate the automated crack repair system, we used 3D-printed crack specimens that mimic real-world crack patterns. These specimens are designed to represent various crack widths, depths, and orientations, providing a robust testing environment for the repair process. The crack specimens are created using a high-resolution 3D printer, ensuring precise replication of different crack geometries. Play Doh mixed with water is used as the filling material due to its ease of testing and reusability. This mixture can be replaced with other materials by simply repeating the calibration setup. The 3D-printed crack specimens are then placed in the testing area, where the robotic system applies the filling material according to the programmed repair procedure.

### **5. Experiments and Results**

This section presents the results of our automated crack repair system, focusing on material extrusion calibration, crack filling efficiency, and the RGB-D camera vs. RGB-D camera-laser localization accuracy. The calibration results demonstrate the relationship between the robot's speed and material extrusion rate, essential for ensuring optimal material flow during repairs. The validation results assess the accuracy of the crack filling process, comparing pre-fill and post-fill profiles to evaluate the system's effectiveness. The crack localization accuracy proves the laser scanner's ability to improve the crack coordinates, instead of relying solely on the RGB-D camera, for successful robot navigation and crack filling. In addition, a video link demonstrating the whole crack filling process can be found [here](#).

#### **5.1 Material Extrusion Calibration**

Accurate material extrusion during crack repair relies heavily on a precise calibration process. To begin, we print a material strip 150 mm in length at a constant robot speed and flow rate. We then use the laser scanner to scan the inner 100 mm of the strip, as the extrusion may be inconsistent at the beginning and at the end of the print. By scanning the middle portion in 10 mm increments, we determine the average cross-sectional

area using the heuristic approach discussed previously. Fig. 11 shows a graph of the print or crack profile where the green and violet circles indicate the indices of the largest sudden change, and the red circle is the center. This process is repeated at different robot speeds to measure the amount of material extruded at each speed, as illustrated in Fig. 12.

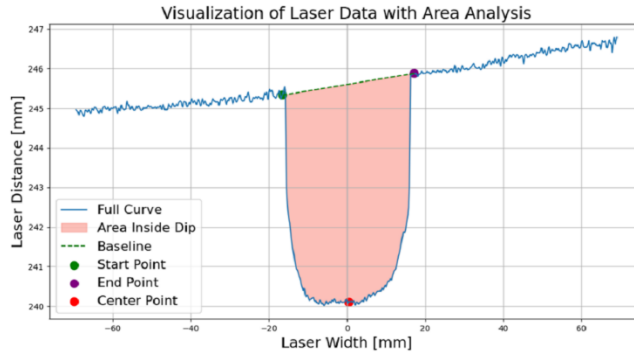


**Fig. 11.** Sample Profile of Calibration Print.

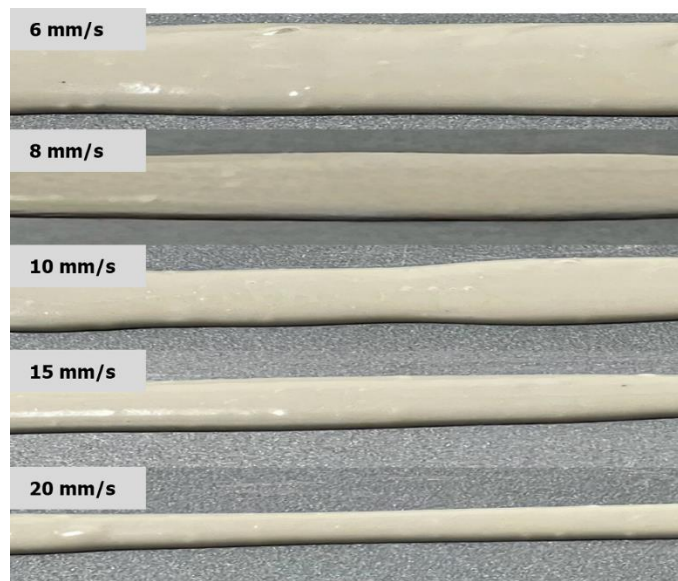


**Fig. 12.** Material Extrusion at Different Robot Speeds.

The calibration process aimed to determine the relationship between the robot’s speed and the amount of material extruded. Various speeds were tested, and the cross-sectional areas of the extruded material were measured. The results, summarized in Table 1, show a clear inverse relationship between the robot's speed and the material extrusion rate: as the robot's speed increases, the amount of material extruded decreases, and vice versa. This calibration allows us to associate specific speeds with their corresponding cross-sectional areas, which is essential for the crack filling process. Each crack coordinate, having varying sizes, requires an appropriate speed for optimal material extrusion.

**Table 1**  
Robot Speed vs. Cross Sectional Area

Robot Speed (mm/s)	Cross-Sectional Area (mm)	Std. Dev. (mm)
6	165.764	18.44
8	111.977	10.807
10	91.448	8.111
15	63.561	7.003
20	41.713	7.936

## 5.2 Crack Filling Efficiency

The accuracy of the crack filling process was evaluated by comparing the pre-fill and post-fill profiles as described in Eq. (11). Table 2 shows the error values  $\epsilon_{fill}$  for various constant speeds, including adaptive speed control. The results indicate that adaptive speed control achieved the lowest error or highest accuracy, with a mean  $\epsilon_{fill}$  of 0.305, a standard deviation of 0.240, and a median of 0.265. In comparison, fixed speeds of 6 mm/s, 8 mm/s, 10 mm/s, 15 mm/s, and 20 mm/s resulted in higher mean and standard deviation values, pointing out less precise filling with a higher degree of overfill or underfill. Fig. 13 demonstrates the qualitative performance of different robot speeds during crack filling, where the adaptive speed shows the least amount of overfill and underfill. Fig. 14 also shows the graph overlay of the crack profile at pre-fill vs. post-fill, which shows the adaptive speed with minimal underfill and overfill. At speed 6 mm/s, there is a large amount of overfill and at speed 20 mm/s, there is a large amount of underfill which is apparent in both Fig. 13. And Fig. 14. The repair process time also varied with speed, with adaptive speed control completing the process in 24.784 seconds, compared to 39.844 seconds for the 6 mm/s speed and 19.102 seconds for the 20 mm/s speed. While the 20 mm/s speed resulted in the shortest repair time, it bargained the filling accuracy, leading to higher deviations in the filled profiles. On the other hand, the adaptive speed control not only provided the most accurate filling but also optimized the repair time by balancing speed and precision. These findings confirm that the automated crack repair system, applying adaptive speed control, can effectively adjust the material flow based on robot speed and deposition based on crack profile data, ensuring accurate and consistent repairs.

**Table 2**  
 $\epsilon_{fill}$  vs. Speed

Speed (mm/s)	Mean <sup>1</sup>	Std. Dev.	Median	Time (s)
6	2.499	3.682	1.186	39.844
8	1.63	2.753	0.387	31.333
10	1.175	2.497	0.221	28.000
15	0.448	0.555	0.265	21.944
20	0.711	0.568	0.608	19.102
<b>Adaptive</b>	<b>0.305</b>	<b>0.240</b>	<b>0.265</b>	<b>24.784</b>

<sup>1</sup>Mean refers to the average from 32 crack coordinates of their  $\epsilon_{fill}$



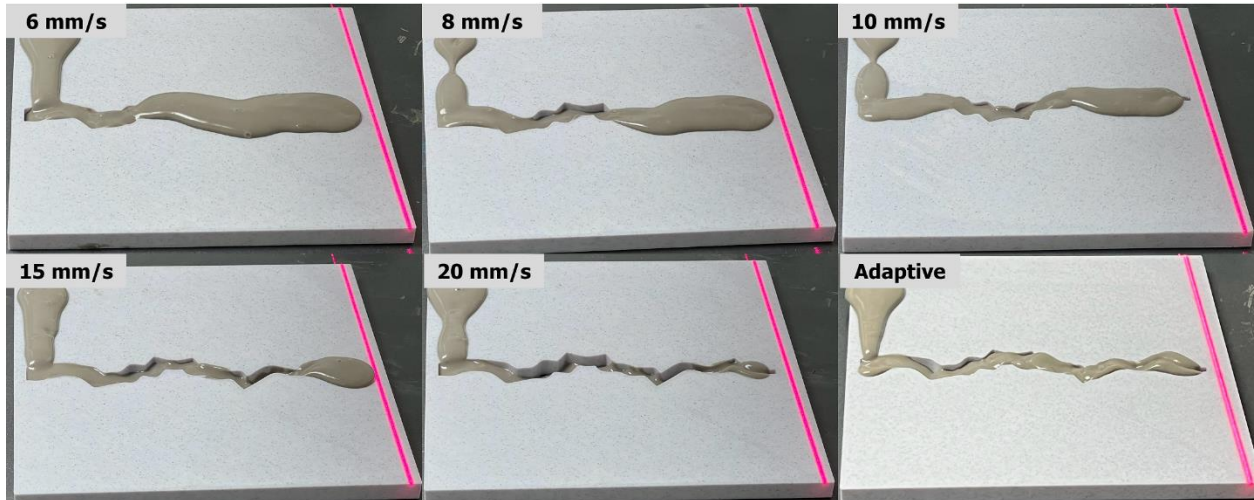


Fig. 13. Filled Crack with Different Speeds.

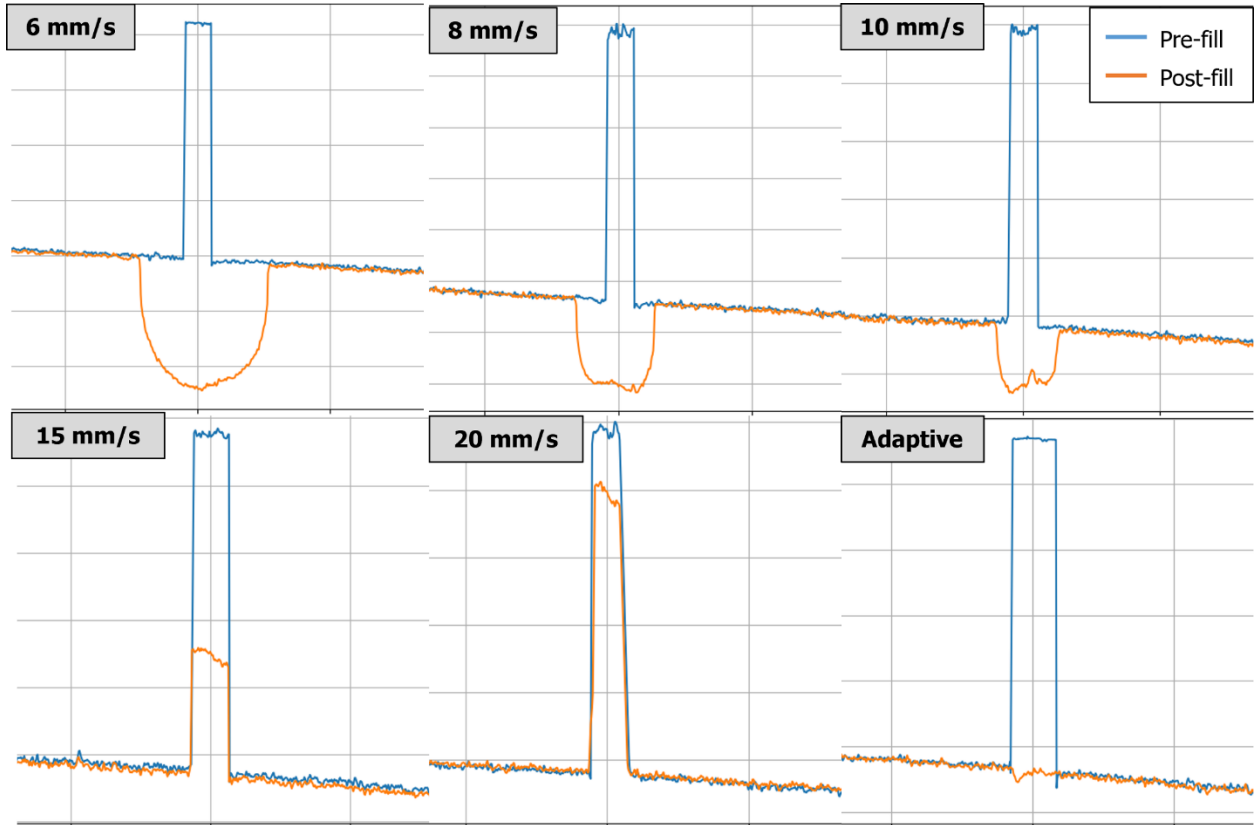


Fig. 14. Visual Overlay of Pre-Fill vs. Post-Fill.

### 5.3 RGB-D vs. RGB-D-Laser Scanner Localization

To illustrate the effect of the addition of the laser scanner on the accuracy of crack coordinate localization, we compare the difference in localization with and without the laser scanner. Experiment 4.2 demonstrated the accuracy of the proposed system with the laser scanner for crack filling. A comparison between the

RGB-D camera-derived coordinates (as described in Section 3.2.4) and those refined by the laser scanner (as detailed in Section 3.3.2) is shown in Table 3 that describes the average differences in the X, Y, and Z coordinates, along with the overall distance difference, assuming that the measurements with the laser scanner are accurate. This analysis is based on 10 complete scans of horizontal cracks, with approximately 24 crack coordinates per scan, totaling over 240 crack coordinates. The results indicate a pronounced change in the estimated location of the crack, particularly in the X and Z coordinates. The X difference initially presented larger inaccuracies due to the horizontal orientation of the cracks tested. This reduction is crucial, as any large error on the X axes could potentially cause the robot to miss the crack entirely, undermining the effectiveness of the repair. Similarly, significant errors on the Z axis can result in improper material deposition, such as inconsistent patterns, due to the substantial height difference between the nozzle and the crack surface. These findings highlight the limitations of relying solely on the RGB-D camera for crack localization, where errors can compromise the effectiveness of crack repair. In contrast, the laser scanner offers a clear enhancement in accuracy, confirming its critical role in ensuring that the robot can achieve precise crack filling.

**Table 3**  
RGB-D vs. RGB-D-Laser Scanner Crack Coordinates Difference

Coordinate	Average Difference (mm)	Std. Dev.(mm)
X	13.575	2.763
Y	0.052	0.033
Z	8.364	2.432
Distance	16.134	2.740

## 6. Conclusion

This paper presents a novel design for an adaptive, autonomous system for surface crack detection and repair using a robotic arm equipped with advanced sensing technologies. The system integrates an RGB-D camera for initial crack detection, a laser scanner for precise crack localization in 3D space and measurements, and an extruder for material deposition. To enable an adaptive repair that significantly enhances repair precision and efficiency, our approach first calibrates the relationship between the robot's speed and material extrusion rate. Then, the system leverages precise crack perception through a combination of RGB-D and laser scanner localization to ensure accurate navigation and optimal material flow tailored to varying crack sizes. Additionally, a novel and repeatable validation approach using a 3D-printed crack was developed. With the novel system design and validation approach, our study clearly demonstrates the benefits of an adaptive system for more efficient and effective filling of cracks compared to a fixed-speed filling. The experimental results confirmed that using the RGB-D camera alone shows the high inaccuracy of crack coordinates in the 10s of millimeters. In addition, another set of experimental results demonstrated the proposed system's capability to perform crack repairs effectively balancing the trade-off between repair time and filling precision. The use of 3D-printed crack specimens and a specially formulated filling material provided a robust and repeatable testing environment, closely simulating real-world conditions. The post-fill validation process, involving laser scanning and fill error calculation, highlighted the system's effectiveness in achieving accurate repairs. This research highlights the potential for adaptive, autonomous systems to significantly improve the quality and efficiency of infrastructure repair maintenance. Autonomous crack repair has the potential for widespread adoption across various infrastructure sectors ranging from residential, commercial, and transportation infrastructure, leading to enhanced safety, reduced maintenance costs, and extended lifespan of critical structures. The introduction of autonomous crack repair technologies represents a pivotal shift in how humans and robots collaborate. HRI systems can take over hazardous, repetitive tasks, thereby reducing the physical strain on workers and allowing them to focus on more complex, judgment-based activities. By minimizing the need for manual labor, this approach not only improves worker safety but also meets the growing demand for automated solutions in infrastructure repair and maintenance.

## Author contributions: CRediT

**Joshua Genova:** Conceptualization, Formal analysis, Investigation, Methodology, Software, Validation, Visualization, Writing – original draft, Writing – review & editing. **Eric Cabera:** Investigation, Methodology, Writing - original draft. **Vedhus Hoskere:** Funding acquisition, Conceptualization, Project administration, Resources, Supervision, Visualization, Writing - original draft, Writing – review & editing

## Declaration of Competing Interest

The authors declare that they have no known competing financial interests or personal relationships that could have appeared to influence the work reported in this paper.

## Data availability

Data will be made available on request.

## Acknowledgements

The authors acknowledge partial financial support from the Department of Defense (Project No. G0511607). The contents of this paper reflect the views of the authors, who are responsible for the facts and the accuracy of the data presented herein. The contents do not necessarily reflect the official views or policies of the sponsors. The authors acknowledge the use of the Carya Cluster and the advanced support from the Research Computing Data Core at the University of Houston to carry out the research presented here.

## *Declaration of Generative AI and AI-assisted technologies in the writing process*

During the preparation of this work the authors used ChatGPT in order to improve readability and language. After using this tool, the authors reviewed and edited the content as needed and take full responsibility for the content of the publication.

## References

- [1] F. Gong, X. Cheng, B. Fang, C. Cheng, Y. Liu, Z. You, Prospect of 3D printing technologies in maintenance of asphalt pavement cracks and potholes, *J Clean Prod* 397 (2023). <https://doi.org/10.1016/j.jclepro.2023.136551>.
- [2] S. Stock, K. Nious, J. Carroll, M. Horn, Sinking, Pooling, Cracking: Runway Problems at San Francisco International Airport Cause More Delays for Travelers, *NBC Bay Area* (2019).
- [3] S. Khakurel, T.Z. Yeow, S.K. Saha, R.P. Dhakal, POST-EARTHQUAKE BUILDING ASSESSMENTS: HOW LONG DO THEY TAKE?, *Bulletin of the New Zealand Society for Earthquake Engineering* 56 (2023) 115–126. <https://doi.org/10.5459/bnzsee.1568>.
- [4] S. Sattar, Recommended Options for Improving the Built Environment for Post-Earthquake Reoccupancy and Functional Recovery Time, Gaithersburg, MD, 2021. <https://doi.org/10.6028/NIST.SP.1254>.
- [5] V. Hoskere, Developing Autonomy in Structural Inspections through Computer Visions and Graphics, University of Illinois at Urbana-Champaign, 2020. <https://www.ideals.illinois.edu/items/117278> (accessed July 20, 2024).
- [6] B.F. Spencer, V. Hoskere, Y. Narazaki, Advances in Computer Vision-Based Civil Infrastructure Inspection and Monitoring, *Engineering* 5 (2019) 199–222. <https://doi.org/10.1016/j.eng.2018.11.030>.

- [7] Z. Yu, Y. Shen, Y. Zhang, Y. Xiang, Automatic crack detection and 3D reconstruction of structural appearance using underwater wall-climbing robot, *Autom Constr* 160 (2024). <https://doi.org/10.1016/j.autcon.2024.105322>.
- [8] J.G. Victores, S. Martínez, A. Jardón, C. Balaguer, Robot-aided tunnel inspection and maintenance system by vision and proximity sensor integration, *Autom Constr* 20 (2011) 629–636. <https://doi.org/10.1016/j.autcon.2010.12.005>.
- [9] B. Sutter, A. Lelevé, M.T. Pham, O. Gouin, N. Jupille, M. Kuhn, P. Lulé, P. Michaud, P. Rémy, A semi-autonomous mobile robot for bridge inspection, *Autom Constr* 91 (2018) 111–119. <https://doi.org/10.1016/j.autcon.2018.02.013>.
- [10] M. Kouzehgar, Y. Krishnasamy Tamilselvam, M. Vega Heredia, M. Rajesh Elara, Self-reconfigurable façade-cleaning robot equipped with deep-learning-based crack detection based on convolutional neural networks, *Autom Constr* 108 (2019). <https://doi.org/10.1016/j.autcon.2019.102959>.
- [11] K. Asadi, H. Ramshankar, H. Pullagurla, A. Bhandare, S. Shanbhag, P. Mehta, S. Kundu, K. Han, E. Lobaton, T. Wu, Vision-based integrated mobile robotic system for real-time applications in construction, *Autom Constr* 96 (2018) 470–482. <https://doi.org/10.1016/j.autcon.2018.10.009>.
- [12] Y. Tian, C. Chen, K. Sagoe-Crentsil, J. Zhang, W. Duan, Intelligent robotic systems for structural health monitoring: Applications and future trends, *Autom Constr* 139 (2022). <https://doi.org/10.1016/j.autcon.2022.104273>.
- [13] M.A.M. Khan, R.W. Harseno, S.H. Kee, A. Al Nahid, Development of AI- and Robotics-Assisted Automated Pavement-Crack-Evaluation System, *Remote Sens (Basel)* 15 (2023). <https://doi.org/10.3390/rs15143573>.
- [14] V. Hoskere, Y. Narazaki, T.A. Hoang, B.F. Spencer, MaDnet: multi-task semantic segmentation of multiple types of structural materials and damage in images of civil infrastructure, *J Civ Struct Health Monit* 10 (2020) 757–773. <https://doi.org/10.1007/s13349-020-00409-0>.
- [15] Q.G. Alexander, V. Hoskere, Y. Narazaki, A. Maxwell, B.F. Spencer, Fusion of thermal and RGB images for automated deep learning based crack detection in civil infrastructure, *AI in Civil Engineering* 1 (2022). <https://doi.org/10.1007/s43503-022-00002-y>.
- [16] Q. Chen, Y. Huang, H. Sun, W. Huang, Pavement crack detection using hessian structure propagation, *Advanced Engineering Informatics* 49 (2021). <https://doi.org/10.1016/j.aei.2021.101303>.
- [17] G. Xu, Q. Yue, X. Liu, Real-time monitoring of concrete crack based on deep learning algorithms and image processing techniques, *Advanced Engineering Informatics* 58 (2023). <https://doi.org/10.1016/j.aei.2023.102214>.
- [18] G. Xu, Q. Yue, X. Liu, Real-time multi-object detection model for cracks and deformations based on deep learning, *Advanced Engineering Informatics* 61 (2024). <https://doi.org/10.1016/j.aei.2024.102578>.
- [19] J. Wang, Z. Zeng, P.K. Sharma, O. Alfarraj, A. Tolba, J. Zhang, L. Wang, Dual-path network combining CNN and transformer for pavement crack segmentation, *Autom Constr* 158 (2024). <https://doi.org/10.1016/j.autcon.2023.105217>.
- [20] J. Dong, N. Wang, H. Fang, W. Guo, B. Li, K. Zhai, MFAFNet: An innovative crack intelligent segmentation method based on multi-layer feature association fusion network, *Advanced Engineering Informatics* 62 (2024). <https://doi.org/10.1016/j.aei.2024.102584>.
- [21] J. Deng, A. Singh, Y. Zhou, Y. Lu, V.C.S. Lee, Review on computer vision-based crack detection and quantification methodologies for civil structures, *Constr Build Mater* 356 (2022). <https://doi.org/10.1016/j.conbuildmat.2022.129238>.
- [22] A. Ji, X. Xue, Y. Wang, X. Luo, W. Xue, An integrated approach to automatic pixel-level crack detection and quantification of asphalt pavement, *Autom Constr* 114 (2020). <https://doi.org/10.1016/j.autcon.2020.103176>.

- [23] D. Kang, S.S. Benipal, D.L. Gopal, Y.J. Cha, Hybrid pixel-level concrete crack segmentation and quantification across complex backgrounds using deep learning, *Autom Constr* 118 (2020). <https://doi.org/10.1016/j.autcon.2020.103291>.
- [24] H. Bae, Y.K. An, Computer vision-based statistical crack quantification for concrete structures, *Measurement (Lond)* 211 (2023). <https://doi.org/10.1016/j.measurement.2023.112632>.
- [25] W. Ding, H. Yang, K. Yu, J. Shu, Crack detection and quantification for concrete structures using UAV and transformer, *Autom Constr* 152 (2023). <https://doi.org/10.1016/j.autcon.2023.104929>.
- [26] A. Ghadimzadeh Alamdari, A. Ebrahimkhanlou, A multi-scale robotic approach for precise crack measurement in concrete structures, *Autom Constr* 158 (2024). <https://doi.org/10.1016/j.autcon.2023.105215>.
- [27] K. Hu, Z. Chen, H. Kang, Y. Tang, 3D vision technologies for a self-developed structural external crack damage recognition robot, *Autom Constr* 159 (2024). <https://doi.org/10.1016/j.autcon.2023.105262>.
- [28] R. Chen, C. Zhou, L. Cheng, Computer-vision-guided semi-autonomous concrete crack repair for infrastructure maintenance using a robotic arm, *AI in Civil Engineering* 1 (2022). <https://doi.org/10.1007/s43503-022-00007-7>.
- [29] F.K.A. Awuah, A. Garcia-Hernández, Machine-filling of cracks in asphalt concrete, *Autom Constr* 141 (2022). <https://doi.org/10.1016/j.autcon.2022.104463>.
- [30] M.E. Torbaghan, B. Kaddouh, M. Abdellatif, N. Metje, J. Liu, R. Jackson, C.D.F. Rogers, D.N. Chapman, R. Fuentes, M. Miodownik, R. Richardson, P. Purnell, Robotic and autonomous systems for road asset management: A position paper, *Proceedings of the Institution of Civil Engineers: Smart Infrastructure and Construction* 172 (2020) 83–93. <https://doi.org/10.1680/jsmic.19.00008>.
- [31] X. Yang, M. Kahouadji, O. Lakhal, R. Merzouki, Integrated design of an aerial soft-continuum manipulator for predictive maintenance, *Front Robot AI* 9 (2022). <https://doi.org/10.3389/frobt.2022.980800>.
- [32] M. Kahouadji, O. Lakhal, X. Yang, A. Belarouci, R. Merzouki, System of Robotic Systems for Crack Predictive Maintenance, in: *2021 16th International System of Systems Engineering Conference, SoSE 2021*, Institute of Electrical and Electronics Engineers Inc., 2021: pp. 197–202. <https://doi.org/10.1109/SOSE52739.2021.9497490>.
- [33] F.R. Pereira, C.D. Rodrigues, H. da S. e. Souza, J.O.C. Neto, M.C. Rocha, G.F. Barbosa, S.B. Shiki, R.S. Inoue, Force and vision-based system for robotic sealing monitoring, *International Journal of Advanced Manufacturing Technology* 126 (2023) 391–403. <https://doi.org/10.1007/s00170-023-11110-z>.
- [34] G. Zhu, Z. Fan, W. Chen, Y. You, S. Huang, W. Liang, R. Fu, J. Xin, J. Chen, F. Deng, Y. Hou, Design and Implementation of a Manipulator System for Roadway Crack Sealing, in: *2019 IEEE 9th Annual International Conference on CYBER Technology in Automation, Control, and Intelligent Systems (CYBER)*, IEEE, Suzhou, China, 2019: pp. 1327–1331. <https://doi.org/10.1109/CYBER46603.2019.9066587>.
- [35] V. Veeraraghavan, K. Hunte, J. Yi, K. Yu, Complete and Near-Optimal Robotic Crack Coverage and Filling in Civil Infrastructure, in: *IEEE Transactions in Robotics*, Institute of Electrical and Electronics Engineers Inc., 2024: pp. 2850–2867. <https://doi.org/10.1109/TRO.2024.3392077>.
- [36] S.D. Schaefer, J. Xu, D. Palin, A. Al-Tabbaa, F. Iida, Position-based fluid simulation for robotic injection sealing of pavement cracks, *J Field Robot* (2024). <https://doi.org/10.1002/rob.22339>.
- [37] M. Rahman, H. Liu, M. Rahimi, C.R. Carcel, L. Kirkwood, I.D. Cardenas, A. Starr, Investigating Precision and Accuracy of a Robotic Inspection and Repair System, 2021. <https://ssrn.com/abstract=3945943>.
- [38] E. Bianchi, M. Hebdon, Development of Extendable Open-Source Structural Inspection Datasets, *Journal of Computing in Civil Engineering* 36 (2022). [https://doi.org/10.1061/\(asce\)cp.1943-5487.0001045](https://doi.org/10.1061/(asce)cp.1943-5487.0001045).

- [39] F. Yang, L. Zhang, S. Yu, D. Prokhorov, X. Mei, H. Ling, Feature Pyramid and Hierarchical Boosting Network for Pavement Crack Detection, *IEEE Transactions on Intelligent Transportation Systems* 21 (2019) 1525–1535. <https://github.com/fyangneil/pavement-crack-detection>.
- [40] Y. Shi, L. Cui, Z. Qi, F. Meng, Z. Chen, Automatic road crack detection using random structured forests, *IEEE Transactions on Intelligent Transportation Systems* 17 (2016) 3434–3445. <https://doi.org/10.1109/TITS.2016.2552248>.
- [41] Q. Zou, Y. Cao, Q. Li, Q. Mao, S. Wang, CrackTree: Automatic crack detection from pavement images, *Pattern Recognit Lett* 33 (2012) 227–238. <https://doi.org/10.1016/j.patrec.2011.11.004>.
- [42] Y. Liu, J. Yao, X. Lu, R. Xie, L. Li, DeepCrack: A deep hierarchical feature learning architecture for crack segmentation, *Neurocomputing* 338 (2019) 139–153. <https://doi.org/10.1016/j.neucom.2019.01.036>.
- [43] M. Eisenbach, R. Stricker, D. Seichter, K. Amende, K. Debes, M. Sesselmann, D. Ebersbach, U. Stoeckert, H.-M. Gross, How to get pavement distress detection ready for deep learning? A systematic approach, in: *2017 International Joint Conference on Neural Networks (IJCNN)*, IEEE, Anchorage, AK, USA, 2017: pp. 2039–2047. <https://doi.org/10.1109/IJCNN.2017.7966101>.
- [44] X. Weng, Y. Huang, W. Wang, Segment-based pavement crack quantification, *Autom Constr* 105 (2019). <https://doi.org/10.1016/j.autcon.2019.04.014>.
- [45] N. Van Oosterwyck, Real Time Human Robot Interactions and Speed Control of a Robotic Arm for Collaborative Operations, (2018). <https://doi.org/10.13140/RG.2.2.28723.53286>.
- [46] RoboDK Inc., RoboDK, (2024).